Over 65% sunlight absorption in a 1 μm Si slab with hyperuniform texture

Nasim Tavakoli,[†] Richard J. Spalding,[‡] Pepijn Koppejan,[†] Georgios Gkantzounis,[‡] Chenglong Wan,[‡] Ruslan Röhrich,[†,¶] Evgenia Kontoleta,[†] A. Femius Koenderink,[†] Riccardo Sapienza,[§] Marian Florescu,[*,‡] and Esther Alarcon-Llado[*,†]

†*Center for Nanophotonics, AMOLF, Science Park 104, NL1098XG, Amsterdam, The Netherlands*

‡*Department of Physics, Advanced Technology Institute, University of Surrey,Surrey, UK*

¶*Advanced Research Center for Nanolithography, Science Park 106, NL1098XG, Amsterdam, The Netherlands*

§*The Blackett Laboratory, Department of Physics, Imperial College London, London SW7 2BW, United Kingdom*

E-mail: m.florescu@surrey.ac.uk; e.alarconllado@amolf.nl

Abstract

Thin, flexible and invisible solar cells will be an ubiquitous technology in the near future. Ultrathin crystalline silicon (c-Si) cells capitalise on the success of bulk silicon cells while being light-weight and mechanically flexible, but suffer from poor absorption and efficiency. Here we present a new family of surface texturing, based on correlated disordered hyperuniform patterns, capable of efficiently coupling the incident spectrum into the silicon slab optical modes. We experimentally demonstrate 66.5% solar light absorption in free-standing 1 μm c-Si layers by hyperuniform nanostructuring. The absorption equivalent photocurrent derived from our measurements is 26.3 mA/cm^2,

which is far above the highest found in literature for Si of similar thickness. Considering state-of-the-art Si PV technologies, the enhanced light trapping translates to a record efficiency above 15%. The light absorption can potentially be increased up to 33.8 mA/cm^2 by incorporating a back-reflector and improved anti-reflection, for which we estimate a photovoltaic efficiency above 21% for 1 μm thick Si cells.

Micrometer-thick silicon photovoltaics (PV) promises to be the ultimate cost-effective, reliable and environmentally-friendly solution to harness solar power in urban areas and space, as it combines the low cost and maturity of crystalline silicon (c-Si) manufacturing[1] with the low weight and mechanical flexibility of thin films.[2–4] Efficient light trapping in ultrathin c-Si is of utmost importance when the film is thinner than the absorption length. Indeed, due to the indirect bandgap of c-Si, inefficient absorption currently hampers the thinning of Si cells below ~ 100 μm, which is crucial to enable flexible, light weight and lower cost c-Si PV.[1,5,6] 3D nanophotonic architectures are crucial for reducing the cell thickness as conventional anti-reflection coatings and multilayers can only prevent light reflection via impedance matching of the solar cell and air, but do not extend the light paths in the Si cell that are required for efficient photon absorption.[7] Despite the fact that many works have focused on nanophotonic principles for enhancing light absorption, there is still no unanimously agreed best strategy for the designing of light trapping nano-textures for PV. Periodic patterning of a thin slab, whether by adding plasmonic[8–12] or dielectric[13–15] structures, can reduce reflection and simultaneously scatter light in the plane of the thin film, but generally work only at discrete wavelengths and specific angle of incidence, due to the discrete crystal momenta of gratings. Oppositely, disordered patterns, such as Asahi roughening or random pyramid etching, scatter the light over a broad angular range and over a large range of wavelengths due to the large rotational and translational symmetry, but are not tailored to match the thin film.[16]

Recently, correlated disordered media have been shown to outperform random roughening and periodic patterning for light trapping.[17–26] Albeit many designs have been presented

so far, it is still an open question what the best design is and whether the optimal one has already been achieved. For instance, it is not obvious if the best result is obtained when starting the optimisation from a periodic or from a random structure. In contrast to these heuristic optimisation methods, hyperuniformity has recently emerged as a new framework to engineer light scattering and diffraction in a rational manner. Hyperuniform disorded (HUD) media are statistically isotropic and possess a constrained randomness such that density fluctuations on large scales behave more like those of ordered solids, rather than those of conventional amorphous materials.[27–30] HUD patterns naturally arise in many physical systems, from the mass distribution in the early universe,[31] structure of prime numbers,[32] hydrodynamics,[33] structure of amorphous ices,[34] sheared sedimenting suspensions,[35] to wave localisation[36] or colloidal packing.[37] When translated into photonic materials, HUDs exhibit large and robust photonic band gaps as in photonic crystals, but are both complete and isotropic.[30] As a result, HUDs display allowed modes that can propagate through the structure in an isotropic fashion as in random media. HUDs are a highly flexible platform to control light transport, emission and absorption in unique ways, beyond the constraints imposed by conventional photonic architectures,[38–42] for the design of freeform waveguides,[43] high-quality factor resonant defects and arbitrarily high-order power splitters,[44,45] hollow-core fibers[46] and photonic bandgap polarizers[47] among others.

In this work we experimentally demonstrate that light absorption in a 1 μm-thick silicon slab is enhanced more than twofold in the wavelength range from 400 to 1050 nm when textured with optimised HUD-based patterns compared to the unpatterned slab. The resulting absorption is the highest demonstrated so far in a Si slab as thin as 1μm. This record value is achieved by k-space engineering of HUD patterns with a tailored scattering spectrum and diffractive coupling of solar irradiation into guided modes of the Si slab. Using our demonstration of light management, we investigate PV efficiency by focusing on the trade-off between light trapping and increased carrier recombination given by the nanotextures. We find that the effect of increased surface-induced charge carrier recombination on the open

circuit potential can be fully compensated by the large photo-currents. A detailed PV efficiency estimation reveals that efficiencies above 20% can be obtained for several optimised HUD designs and state-of-the-art Si PV technologies. This is a highly remarkable efficiency for such a thin indirect-bandgap material, which together with the fact that lower grade raw Si material can be used in such thin devices, establishes a new breakthrough in thin light-weight and flexible solar cells.

Light absorption in films with disordered hyperuniform patterns

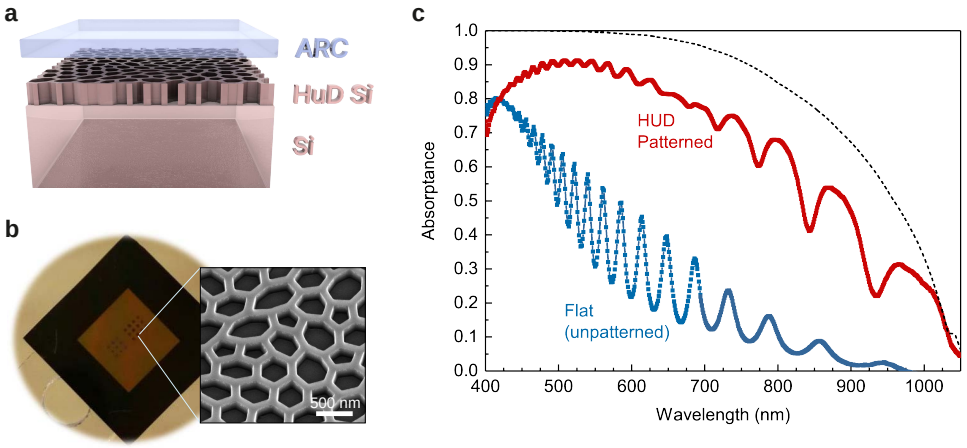

Fig. 1 Ultra-thin light absorber design. **a** Schematic representation of the ultra-thin light absorber consisting of a 1 μm-thick silicon film with the HUD pattern on the top surface ($\sim$ 200 nm thick) to improve light trapping. The pattern is infiltrated with a lower refractive index material (n_{LRM}), which is also used in a top flat layer, ARC, to reduce reflectance (50-100 nm in thickness). Note that the ARC layer is depicted floating above the nanopattern in the image only for clarity purposes **b** Optical image of the silicon membrane sample supported by a thick silicon frame (1×1 cm^2), where the textures have been fabricated. Inset: Scanning electron image of the as-fabricated Si membrane with the optimized honeycomb-like HUD network pattern. **c** Absorptance spectra measured for the Si membrane with (red) and without (blue) the HUD pattern with ARC. The membrane is suspended in air and infiltrated with a polymer resist ($n_{LRM} = 1.52$) as ARC. The dashed black line corresponds to the Lambertian limit absorption for 1 μm Si, based on the optical properties given in Ref. 48.

We demonstrate the power of hyperuniform disordered (HUD) patterns for lightweight, flexible and efficient photovoltaics, by first focusing on the absorption properties in ultrathin ($\sim$ 1 μm) Si. The proposed structure for the highly efficient Si light absorber is shown in

Fig. **1**a. It consists of a thin Si slab (1 μm), of which the top 200 nm is patterned with an optimised HUD pattern. In this case, the pattern consists of a 2D network of Si walls, that resembles the honey-comb underlying structure in black butterfly wings.[24,49] The Si pattern is infiltrated with a low refractive index medium by spin coating a polymer resist [50] with refractive index of 1.52. While the infiltrated pattern layer is expected to also reduce reflectance due to the better index matching with air ($n_{pattern} \approx n_{Si} \cdot f + n_{LRM}(1-f)$, with f being the Si filling fraction), an additional layer of resist on top ($50-100$ nm thick) further improves anti-reflectance, referred to as ARC. While the optical properties of the resist are not the ideal to guarantee minimal reflection, spin coating is a simple conformal fabrication method that ensures nanopattern filling and a flat top surface. Fig. **1**b is a photograph of a suspended 4.8×4.8 mm^2 Si membrane nominally 1 μm-thick on a Si support frame before spin coating the resist. The membrane reveals a semi-transparent reddish colour owing to its small thickness and small absorption coefficient in the red and near infra-red. HUD-based patterns were fabricated on the membrane with e-beam lithography in at least 100×100 μm^2 areas. These areas are clearly visible in the picture as they appear darker, highlighting the increased light trapping. A close-up scanning electron microscopy (SEM) image of the fabricated HUD network pattern on the Si suspended membrane is shown as inset.

We have measured the light absorption of the free-standing membrane with ARC on the unpatterned and patterned regions by using an integrating sphere microscope.[51,52] The curves in Fig. **1**c compare the light absorption as measured for the flat membrane with that of the HUD patterned membrane. The absorption spectrum of the flat membrane shows the characteristic Fabry-Pérot interferences for a 1.18 μm thick Si slab (see Supplementary Information), with a peak in absorption at about a wavelength of 450 nm and rapidly decreasing absorption for longer wavelengths due to the small absorption coefficient of Si in the visible and near infra-red. In contrast, the absorption in the membrane with the HUD pattern is on average 50% higher in absolute numbers for the wavelength range of 500 to 900

nm and it follows the Lambertian limit trend ($4n^2$ limit for 1 μm-thick Si represented by the black dashed curve), which does not take into account reflection losses. Despite the fact that the membrane sits in air (i.e. no back-reflector) and the sub-optimised ARC, the fraction of absorbed solar photons in the membrane increases from 25.5% to 66.5% by texturing the surface based on our optimised HUD design. This is the highest demonstrated absorption in a 1 μm Si absorber so far, and translates to a photocurrent of 26.3 mA/cm^2, far above the 19.72 mA/cm^2 in the best reported cell with similar thickness.[53] Simulations show that a metal back reflector will increase absorption even further for the whole spectrum and integrated absorption can reach up to 93.4% of the Lambertian absorption. In the following, we describe the design principle and physical mechanism that induces this record in absorption.

Light trapping mechanism and design optimisation

As in previous works that use periodic and heuristic aperiodic structures to promote light trapping, the main mechanism by which the HUD nanostructure enhances absorption is diffraction into the absorber.[17,54,55] In the presence of texturing, the guided modes of the thin silicon slab become leaky (quasi-guided) and can in- and out-couple to the incoming electromagnetic modes supported by the surrounding medium. The waveguide mode dispersion for a Si slab is shown in Fig. **2**a, where we note that within the spectral region of interest, c-Si exhibits strong dispersion that leads to a strong curvature of the Si light cone and significantly different absorption of the guided modes, as indicated by the color scale in Fig. **2**a. The total absorption is given by summing up the coupling contributions of each mode. To maximize sunlight absorption in the slab we need to couple efficiently to these lossy modes that exist for $k_{\|}$ above the light-cone of air (*lower black thick curve*), for a broad range of wavelengths (from 350 nm to 1100 nm). Due to the large number of modes in a 1 μm Si slab, a pattern structure that diffracts incident light ($k_{\|} = 0$ for normal incidence) to the range of $k_{\|}$ from $\sim$ 15 to $\sim$ 20 μm^{-1} (indicated by the two horizontal dashed lines in Fig. **2**a) ensures all sunlight has a mode to couple to. However, due to the inhomogeneous

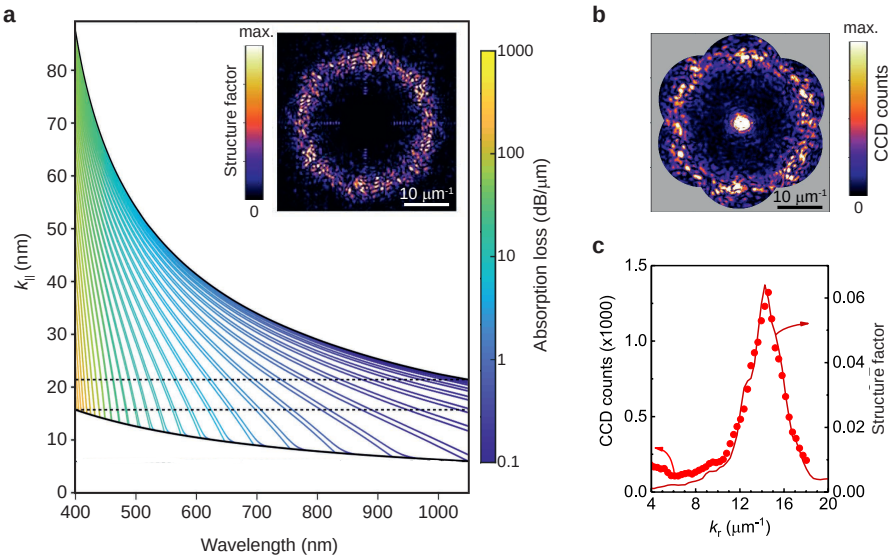

Fig. 2 Light trapping mechanism. **a** Waveguide modes for a homogeneous 1μm thick Si slab between air and a perfect metal for the wavelength range of interest in a solar cell. The modes are all lossy, with the absorption loss denoted by their color, as shown in the color bar. Black lines denote the dispersion curves for air (lower curve) and for Si (upper curve). The horizontal dashed lines denote two characteristic wavenumbers: $k_1 = 15.71$, and $k_2 = 21.41$ μm^{-1} as described in the text. Inset: Simulated first order diffraction pattern of the HUD network design that shows a characteristic diffraction ring in the desired k-space. **b** Measured Fourier-space diffraction pattern in reflection of the *HUD network* design lithographically patterned in a Si wafer (wavelength 561 nm). **c** Structure factor based on the radial distribution of the diffraction intensity in **a** and **b**.

absorption of the guided modes, coupled-mode theory calculations estimate that the highest absorption is actually given for uniform diffraction to the k-range from ~ 9 to ~ 25 μm^{-1} (see the detailed calculation in the Supplementary File). Targeting this wave vector range is a key design goal for engineering the diffraction pattern.

In contrast to periodic and random patterns, hyperuniform designs with correlated disorder are an intermediate concept that allows the creation of diffraction into only a tailored range of wavevectors. In particular, stealthy HUD structures offer a distinctive route to filling desired bands in Fourier space, intermediate between the continuous k-space content of random patterns, and the discrete crystal momenta of periodic point patterns. Stealthy HUD point patterns are isotropic with no diffraction below a certain critical wavevector value, k_C: $S(k_{||} \leq k_C) = 0$). The so-called stealthiness parameter χ is defined as the frac-

tion of wavevectors for which the structure factor vanishes and can be used to measure the hyperuniform correlations. Thus, $\chi = 0$ for purely uncorrelated (Gaussian) point patterns and $\chi > 0.77$ for periodic structures.[28,36,38,42]

Our design approach starts with a 2D HUD point pattern ($\chi \sim 0.4 - 0.5$) that provides the most uniform filling in the Fourier space domain delimited by the two wavenumbers ($k_{\parallel,1}$ and $k_{\parallel,2}$) estimated from the waveguide properties of the slab. Once the 2D HUD point pattern is created, it is transformed into a physical 3D design that can be fabricated with two material components: Si and the low refractive index material. In this case, the 2D HUD point pattern is decorated with 200 nm tall Si walls following a Delaunay tesselation protocol[38] that form a continuous Si network, and the voids are filled by the low refractive index material. However, with this design light absorption is no longer expected to be optimal as the 3D texture strongly disrupts the waveguide properties of the Si slab. Also, the tesselation protocol causes the resulting 3D network to be nearly hyperuniform as it slightly deviates from hyperuniform,[56] meaning that its structure factor has some amplitude for $k_{\parallel} < k_c$.

To resolve this non-ideality, we introduce a second optimisation step to fine-tune the HUD-based 3D pattern, where the HUD properties (average distance between points) and Si filling fraction are optimised. This is done with full-wave 3D numerical simulations that compute light absorption at each optimisation step (see Methods and Supplementary File). While the process is computationally expensive, the initial 2D HUD optimisation procedure sets a good base to rapidly find a local maximum. As a result, we obtain an optimised 3D structure based on a 2D HUD point pattern, but with a structure factor function that may differ from what was initially estimated from the slab waveguiding properties. The inset in Fig. **2**a shows the 2D simulated structure factor of the fully optimised HUD network design that was used to create the sample in Fig. **1**. The structure factor for the first order diffraction shows a clear fingerprint of the hyperuniformity with a circular region around $k_{\parallel} = 0$ where $S(k)$ vanishes, but there is not a sharp cut-off as initially imposed. The nearly-

hyperuniform structure factor is better discerned in the angle-averaged structure factor (solid curve) shown in Fig. **2**c. Notice that the Fourier space in the optimised pattern is filled in the wavevector region between 12 and 17 μm^{-1}, which is slightly different than the initial guess for $k_{\parallel,1}$ and $k_{\parallel,2}$.

We have performed momentum spectroscopy of the fabricated pattern on a Si surface, where the measured k-space diffraction pattern in reflection is shown in Fig. **2**b as obtained using high-NA Fourier microscopy.[57] By construction the HUD pattern is designed to scatter normally incident light to parallel wave vectors that are *outside* the collection NA of air objectives. However, by combining strongly off normal illumination at six azimuthal angles we can reconstruct the structure factor in 2D Fourier space up to an effective NA almost twice higher than that of the objective lens (see full details in the Methods section). The angle resolved diffraction measured in reflection displays a similar fingerprint of the hyperuniformity as the 2D structure factor of the design. The measured angle-averaged reflection is also plotted in Fig. **2**c, and is extremely well reproduced by the theoretical structure factor (solid line).

Comparison of HUD-based designs.

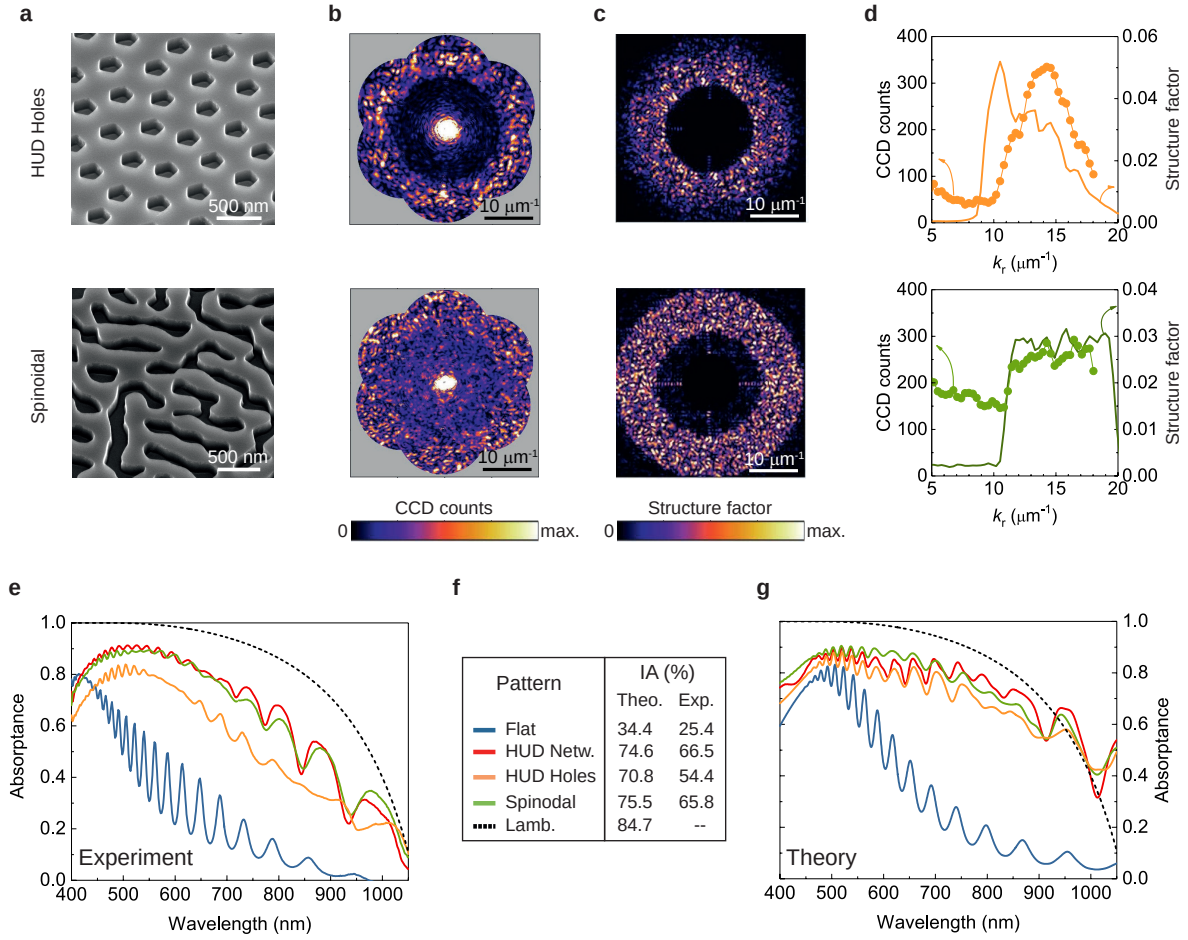

Fig. 3 Performance comparison between different HUD-based designs. **a** SEM images of samples textured with the *HUD hole* (top) and *spinodal* (bottom) designs. **b** Measured angle-resolved diffraction in reflection of the corresponding pattern. **c** Simulated 2D structure factor for the optimised *spinodal* and *HUD hole* patterns. **d** Structure factor as a function of in-plane wavevector (k_r) given by the angle-averaged simulated (solid curve) and measured (dots) diffraction. Measured (**e**) and calculated (**g**) absorptance spectra for a 1μm thick Si slab suspended in air with the different surface nanopattern designs with ARC considered. The absorption spectrum for the *HUD network* design is the same as in Fig.**1**.The theoretical Lambertian limit and the absorption for a flat Si slab (with an ARC) are shown as reference. **f** Table listing the percentage of integrated absorbed solar photons (IA) for all patterns for the wavelength range of $400 - 1050$ nm. These numbers are obtained by integrating the theoretical or experimental absorption spectra over the solar flux (AM1.5G) and normalising for the total photon flux in the specified wavelength range.

So far, we have shown that a 2D HUD point pattern can lead to a highly efficient 3D design for broadband light trapping in a thin Si slab, by *decorating* the point pattern with two

materials in a wall network fashion (Fig. **1**b). However, there are many other decorating possibilities for the same initial 2D HUD pattern. For instance, instead of the wall network, one could place Si nano-pillars or nano-holes at the points of the 2D HUD point pattern and fill the voids with ARC. This is the simplest HUD design, where a single element is cloned at tailored positions. We refer to this texture as *HUD hole*, and the SEM image of the as-fabricated sample is shown in Fig. **3**a. Similar to the *HUD network* in Fig. **1**, the Fourier microscopy intensity map, Fig. **3**(b,top), indicates the HUD nature of the the design and it is very similar to the theoretical structure factor, Fig. **3**(c,top).

Another very different way of obtaining 3D HUD patterns is inspired by the generation of *spinodal* structures.[58,59] Here the mathematical recipe is to first define a random superposition of cosine waves with random phase, with wave vectors imposed by the desired wave vector distribution ($k_{\parallel,1} \leq k_{\parallel} \leq k_{\parallel,2}$), or structure factor. Thresholding the resulting function at a fixed height value defines material boundaries separating Si and low refractive index material (filling fraction f set by threshold choice), tracing out zebra-like patterns as in Fig. **3**(a, bottom). The resulting two-phase material pattern is nearly hyperuniform, for which its structure factor is dominated by the wave vector distribution imposed at the initial design stage. Owing to its inspiration, we refer to this design as *spinodal*. Fourier microscopy of the as-fabricated *spinodal* design, Fig. **3**(b, bottom), also exhibits a characteristic low scattering at small wavevectors, and a marked increase of scattering at $k_{\parallel} \sim 11\ \mu\mathrm{m}^{-1}$. The contrast is lower compared to the other HUD designs and the scattering at small wavevectors is not expected from the theoretical structure factor, Fig. **3**(c, bottom). We suspect the additional scattering at low wavevectors arises from fabrication imperfections.

The azimuthally-averaged k-space resolved diffraction and theoretical structure factor for the *HUD holes* and *spinodal* designs are shown in Fig. **3**d as dots and solid lines, respectively. While the intensity distribution in the structure factor of the *HUD holes* is similar in shape to that of the *HUD network* pattern with a peak at $\approx 15\ \mu\mathrm{m}^{-1}$, the structure factor of the *spinodal* is quite different and resembles a square function. All three proposed designs

have a structure factor that is well suited to couple normally incident sunlight into the plane for absorption. The theoretical and experimental absorption spectra for the patterned and unpatterned suspended membranes are shown in Fig. **3**e and g, where the ARC (same parameters for all designs) is also taken into account. The spectrum for the *HUD network* pattern is also included and it is the same as in Fig. **1**c As a quantitative measure to compare absorption between all the different designs, we have computed the fraction of absorbed solar photons (integrated absorption, IA), as listed in the table in Fig. **3**f. The IA, is computed by considering the AM1.5G solar spectrum for the wavelength range of 400 to 1050 nm (see the Methods section for more details). For comparison, we also plot the Lambertian limit obtained by considering the same optical constants used in the full-wave simulations. Similar to the spectra measured in the *HUD network* patterned membrane (red curve), the two new designs raise light absorption in the long wavelength regime, particularly in the case of the *spinodal* (green curve). As expected from the absorption spectra, the *spinodal* and *HUD network* patterns result in a similar IA ($\sim 66\%$ in practice and $\sim 75\%$ in theory). As also predicted by theory, the *HUD holes* design leads to a slightly lower absorption and IA ($\sim 54\%$ in practice and $\sim 70\%$ in theory). We attribute the discrepancy between theory and experiment to local deviations in the ARC and membrane thickness. In any case, for all three designs the measured IA is more than twice that of the unpatterned membrane and we experimentally demonstrate for the first time and for two patterns that absorption is as high as $\sim 78\%$ of the Lambertian limit.

Full device design and efficiency estimation.

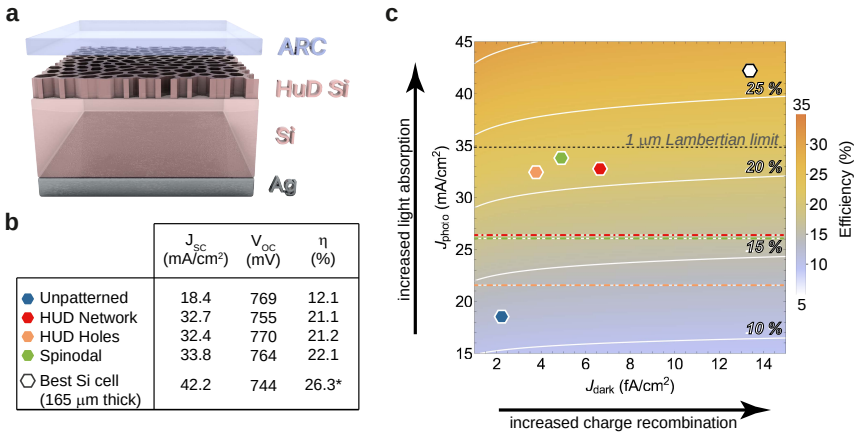

	J_{SC} (mA/cm^2)	V_{OC} (mV)	η (%)
Unpatterned	18.4	769	12.1
HUD Network	32.7	755	21.1
HUD Holes	32.4	770	21.2
Spinodal	33.8	764	22.1
Best Si cell (165 μm thick)	42.2	744	26.3*

Fig. 4 PV efficiency estimation. **a** Full solar cell device design, which includes a Ag back-contact and improved ARC ($n_{LRM} = 1.82$ and 72 nm thick) **b** Table summarising the estimated PV performance parameters from our optical and PC1D device simulations. **c** Color-map indicating the non-linear dependence of the maximum PV efficiency on the dark and photo-currents (J_{dark} and J_{photo}, respectively). The white lines are isolines at the efficiency indicated by the labels. The dashed black line corresponds to the J_{photo} given by the Lambertian limit in a 1 μm-thick Si slab. The dash-dotted lines correspond to the J_{photo} derived from our absorption measurements without back-reflector. The data points correspond to the estimated PC1D efficiencies for the different designs. The efficiency estimated for the unpatterned Si membrane and that for the best demonstrated bulk Si cell are shown for comparison. The total efficiency is not only affected by increased light trapping, but also by the additional pattern-induced surface area recombination, reflected in the increased dark current.

So far, we have demonstrated the exceptional light trapping properties of the HUD patterns in thin Si, as evidenced by the enhanced absorption. However, in a full solar cell device one must also consider other effects of nanotexturing on its performance. It is important to assure that the gain from light trapping for PV remains despite the potential penalty of increased surface recombination, which can strongly affect the performance of devices with a Si thickness smaller than ~ 90 μm, where bulk-related losses are negligible. In order to understand the effects of our HUD-based designs on the PV efficiency, we consider the full device structure shown in Fig. **4**a. Now, the patterned Si film sits on top of a silver metal contact that also acts as a back reflector. By using interdigitated macroscopic Ag pads, both the n and p contacts are placed at the rear which reduces shading on the front of the cell.

This technology, known as interdigitated back contact (IBC) photovoltaics, has enabled the highest PV efficiency in Si-based cells.[60–62] For simplicity, in our absorption calculations we consider a continuous Ag film at the back instead of the interdigitated pads, which is a fair assumption for optical purposes given their large characteristic sizes.

We have re-optimised the 3D pattern design taking into account the Ag back-reflector as part of the full structure. We also consider an improved ARC configuration, with $n_{LRM} = 1.82$ and ARC thickness of 72 nm (see Supplementary Information). The resulting absorption spectra for all the different designs are shown in the Supplementary Information. As expected, the metal back-reflector and improved anti-reflection increases light absorption as compared to that shown in Fig. **3**g. Interestingly, the three designs offer a highly robust absorption to changes in the angle of incoming light (see the angle dependent absorption spectra in the Supplementary Information file), which strongly enhances the daily PV power output.

We have computed the photocurrent, J_{photo}, by integrating the simulated absorbed solar spectrum for the wavelength range of 300 to 1050 nm. To estimate the PV efficiency of our designs we have simulated the current-voltage characteristics of the solar cell with the PC1D software, where we have considered J_{photo} as input and a bulk lifetime of 0.5 ms (standard PV grade Si) and surface recombination velocity (SRV) of 100 cm/s. The SRV value is the state-of-the-art in high efficiency Si solar cell devices.[1,60] In order to account for the pattern-induced increased surface area, we have considered an effective SRV by multiplying it by the surface area increase factor. A more detailed description of the parameters used in our simulations is given in the Supplementary Information. The table in Fig. **4**b summarizes the estimated solar cell performance, in terms of short circuit current (J_{SC}), open circuit potential (V_{OC}) and PV efficiency (η), for the optimised *HUD hole*, *HUD network* and *spinodal* patterns. For comparison, we have included the theoretical case of an unpatterned Si membrane (with ARC) and the current record Si cell, which is 165 μm thick.[60]

Because we assume no external resistance losses, $J_{SC} = J_{photo}$. With the pattern-induced

light trapping, the J_{SC} in 1μm-thick Si is almost doubled for all three designs compared to the unpatterned cell (from 18.5 mA/cm^2 to 33 mA/cm^2), close to the Lambertian value for 1 μm-thick Si (at 35 mA/cm^2). At the same time, the estimated V_{OC} values in our three designs are higher than the best bulk cell and oscillate around that expected in an unpatterned thin film. Because of the small volume in a 1μm film compared to bulk, the saturated dark current, J_{dark}, in the cell is only limited by surface recombination. Considering the state-of-the art bulk carrier lifetime and surface recombination velocity, J_{dark} is almost one order of magnitude smaller in a 1μm Si film compared to Si bulk (165 μm thick) and thus the V_{OC} is improved by thinning Si down.[1,5,63] An interesting consequence of this is that lower grade Si material can thus be used in such thin devices, which have much lower costs (see the Supplementary Information for more details on how the PV efficiency is affected by the bulk lifetime and surface recombination). As V_{OC} also depends on the photocurrent, J_{photo}, light trapping has the potential to compensate the effects of patterning-induced larger J_{dark} on the voltage. We find that, the *HUD holes* design uses the smallest surface area and the strong light trapping fully compensates the effect of increased surface recombination and leads to the same V_{OC} as in the unpatterned case.

From the PC1D full current-voltage characteristics we obtain the PV efficiency. Despite the different light trapping power and texture design in all three 1 μm-thick Si patterned cells, we estimate their solar cell efficiency to break the 20% milestone. Fig. **4**c represents the two major consequences of nanotexturing, increased light trapping and increased charge recombination, on the PV efficiency (color scale) by considering the illuminated diode equation ($J(V) = J_{dark}(e^{qV/K_BT} - 1) - J_{photo}$). The dashed horizontal black line corresponds to the ultimate photocurrent from the Lamertian light trapping in 1 μm thick Si and one can see the span of possible PV efficiencies depending on the carrier recombination properties of the device. In the graph, we include data points for the unpatterned and the three HUD designs, based on the J_{photo} and J_{dark} values found in our light absorption and PC1D simulations, respectively. For comparison, we also include the data point for the best demonstrated Si

solar cell, which is 165 μm thick.[60] Note that the diode equation yields a slightly higher PV efficiency compared to that reported in Ref.60 (0.5% higher efficiency) as the model neglects contact resistance losses. Fig. **4**c clearly visualizes the compromise for the total efficiency between light trapping and surface recombination properties of the different designs and it is particularly evidenced by the *HUD holes* and *HUD network*. Despite the fact that the two designs have different light trapping capabilities, the final PV efficiency is very similar.

While we theoretically predict the ultimate best device to be that with the *spinodal* texture, the large scale implementation of its fabrication may require some further technological developments. A combination of interference and nanoimprint lithography[64] has already demonstrated the fabrication of aperiodic structures with defined spatial frequency distribution in areas larger than 1 m^2. However, further work is needed to increase the required patterning resolution down to few tenths of nanometers. By contrast, HUD point patterns naturally arise in many physical systems, that can lead to simple and scalable fabrication of the *HUD holes* or *HUD network* patterns. For instance, it has been shown that the structure factor of dispersed colloidal particle (e.g. beads) patterns can be tuned by the ionic strength of the particular solvent[65,66] and that the dewetting of semiconductor layers leads to HUD patterns.[67] Also, soft-imprint conformal lithography has proven an excellent low-cost alternative to pattern large-areas with a resolution below 10 nm that could actually serve for both *HUD holes and HUD network*.[68] While a master substrate has to be first made with other lithography methods (such as e-beam lithography), the master can be extensively re-used for the creation of multiple-use soft stamps.

Conclusion

We have shown that stealthy HUD point patterns are an excellent platform to design a wealth of highly efficient nanoscale textures for trapping light in ultrathin Si solar cells. We have described three different texture designs that offer broadband isotropic light trapping with a characteristic hyperuniform signature in the Fourier reflectance. We have fabricated

such textures on a suspended Si membrane and experimentally demonstrated the highest absorption in 1 μm-thick Si, corresponding to a J_{photo} of 26.3 mA/cm^2. This exceptional light trapping can potentially be further improved by optimising the anti-reflection coating and incorporating a metal back-reflector, which in turn serves as electrical contact. Taking into account state-of-the-art values of Si electronic properties and IBSC device design, we estimate realistic PV efficiency above 21% for a 1 μm-thick c-Si cell, which represents a breakthrough toward flexible, light-weight c-Si PV.

Methods

Generation of the disordered Hyperuniform structures

A hyperuniform point pattern is a random point pattern in real space for which the number variance $\sigma^2(R)$ within a spherical sampling window of radius R (in d dimensions) grows more slowly than the window volume ($\propto R^d$) for large R. We consider point patterns that are stealthy, which is a property of the structure factor S(k), defined as[27]

$$S(\mathbf{k}) = \frac{1}{N}\left|\sum_{n=1}^{N} e^{i\mathbf{k}\cdot\mathbf{r}_n}\right|^2 , \tag{1}$$

where $\mathbf{k}$ are vectors in reciprocal space and $\mathbf{r}_n$ are the positions of the N particles. For stealthy point patterns, $S(\mathbf{k})$ is isotropic and vanishes for a finite range of wave numbers $0 < k \leq k_0$, for some positive critical wave vector, k_0.[29] The size of this region can be expressed through the so-called stealthy parameter $\chi = M(\mathbf{k})/dN$, where $M(\mathbf{k})$ is the number of linearly independent $\mathbf{k}$ vectors where $S(\mathbf{k}) = 0$ and $d = 2$ in the present case.[29,38]

Generation of the spinodal pattern

Density wave (spinodal) structures or spinodal structures are a particular realization of hyperuniform structuring and can be generated according to a simple protocol.[58] We consider

the function

$$\Phi(\mathbf{r}) = \sum_{j=1}^{N_q} \cos(\mathbf{q}_j \cdot \mathbf{r} + \phi_j) \ , \tag{2}$$

where $k_1 < |\mathbf{q}| < k_2$ is a collection of *homogeneously* distributed random N_q wavevectors and ϕ_j are random phases uniformly distributed in the range $(0, 2\pi)$. This function is hyperuniform by construction with its Fourier transform uniformly distributed in the k-space ring defined by $k_1 < |\mathbf{q}| < k_2$. To obtain a two-phase dielectric function we define

$$\epsilon(\mathbf{r}) = \begin{cases} \epsilon_1 \ , \Phi(\mathbf{r}) < \Phi_0 \\ \\ \epsilon_2 \ , \Phi(\mathbf{r}) \geq \Phi_0 \end{cases} \ , \tag{3}$$

where ϵ_1 and ϵ_2 are relevant dielectric permittivities of the two phases, and Φ_0 is a value chosen to yield the desired filling fraction. We note the cut procedure defined above may violate the strict hyperuniformity constraints, and in practice the resulting structures are nearly-hyperuniform with most of the Fourier components concentrated in the k-space ring defined by $k_1 < |\mathbf{q}| < k_2$.

Absorption simulations

Optical simulations were performed using the a freely available finite-difference time-domain (FDTD) solver.[69] In all cases, the disordered structures were generated under periodic boundary conditions and are modelled as super-cells with sizes between 10 - 15μm. For absorption simulations, we have employed periodic boundary conditions in the transverse directions and perfect matching layer boundary conditions in the longitudinal direction. The dispersive dielectric function of Si was modeled using a sum of Lorentzian terms[23] as detailed in the Supplementary Information and the mesh resolution was 5.2 nm. To calculate the absorption, the structure was illuminated by broad bandwidth plane waves pulses, and the subsequent transmitted and reflected fluxes were recorded for a long simulation time. Due to the diffusive character of the wave propagation and presence of various localised resonances

in the disordered texture layer, the simulation is not run for a fixed amount of time but it keeps running until the field in the slab have decayed by a factor of 5×10^{-5} from its peak value in an interval of 20 simulation time units.[69]

Sample fabrication

Single crystal $\langle 100 \rangle$ 1μm Si membranes (Norcada Inc.) were used. The actual thickness of the membrane may vary slightly. From the Fabry-Pérot interference pattern in the absorption spectrum for the unpatterned membrane nearby the patterned areas, we deduce a total thickness of 1180 nm. The membranes were either 1.3×1.3 mm^2 or 4.8×4.8 mm^2 in size in a Si frame of 10×10 mm^2 and 300 μm thick. The nanopatterns were made by electron beam lithography followed by reactive ion etching. First, CSAR e-beam resist was spin coated as mask. Fields of either 100×100 , 150×150 or $180 \times 180 \mu$m^2 patterns were exposed. After exposure and development, 200 nm of the Si membrane was etched by first removing the native oxide followed by HBr and O_2 etching. The left-over resist was lifted off, and the sample was ready for Fourier microscopy. For the absorption measurements, an additional layer of resist (OrmoComp® resist) was spin coated on top of the sample to act as anti-reflective coating, ARC. The effects of the ARC on light absorption are described in the Supplementary Information. From the interference fringes in the absorption spectrum taken on the unpatterned area, we deduce that the resist layer is of 200 nm.

Fourier-space illumination and imaging

In order to experimentally characterize the structure factor of the hyperuniform structures, we employed high-NA back focal plane imaging, also known as Fourier microscopy. In this technique angle-dependent scattering patterns of a sample are captured in single shot measurements, as opposed to performing angular scans using a rotation stage. We used a home-built inverted microscope reported in Ref.[57] that operates in reflection mode, so we chose the structures on the Si wafer for these measurements for easier handling. The

microscope is infinity corrected with an Olympus MPlan IR 100x NA=0.95 objective, a 200 mm tube lens and 200 mm Fourier lens.

As the light source we use a cw DPSS laser (Lasos DPSS) with a wavelength of 561.3 nm. At this wavelength, the actual microscope NA equals 0.89, as calibrated with a diffraction grating. The image of the objective back focal plane is relayed to an Andor Clara silicon CCD camera. According to the Abbe sine condition, captured Fourier images directly map parallel momentum space, as scattering at angle θ, ϕ (polar angle relative to sample normal and azimuthal angle, respectively) projects onto the camera plane at location $(x, y) = f_o(\cos\phi \sin\theta, \sin\phi \sin\theta) \propto \mathbf{k}_{||}$, where f_o is the microscope objective focal length (f=1.8 mm). Since we essentially measure the structure factor as function of $k_{||}$ (wave vector parallel to the Si/air interface), one would expect to see the same dependence in both reflection and transmission.

Essential to our experiment is that the HUD patterns have structure factor $S(\mathbf{k}_{||})$ predominantly at parallel momentum *just outside* the NA of our collection objective, corresponding to scattering normally incident light into guided modes. The ring of diffraction intensity distribution in momentum space follows $I(\mathbf{k}_{||}) = S(\mathbf{k}_{||} - \mathbf{k}_{\mathrm{in},||})$ and is therefore centered on the incident parallel momentum $\mathbf{k}_{\mathrm{in},||}$. From free space one can therefore access the structure factor $S(\mathbf{k}_{||})$ for parallel momenta up to *twice* the microscope NA by illuminating at multiple oblique incidence angles [$0 < \frac{|\mathbf{k}_{\mathrm{in},||}|}{2\pi/\lambda} \approx \mathrm{NA}$].

In order to access any excitation angle without physically moving parts of the set up, the excitation path is equipped with a spatial light modulator (Meadowlark 1920 × 1152 XY Phase Series SLM) that is imaged onto the microscope back focal plane. By displaying regions of blazed phase gratings on the SLM, light can be selectively send to the first grating order. This allows an effective amplitude modulation, by placing an iris in the Fourier plane of the SLM, which blocks all light except for the modulated first diffraction order.[70] By displaying a single small circle on the SLM and choosing its position, illumination with arbitrarily $\mathbf{k}_{\mathrm{in},||}$ can be generated. For each structure we collected six images arranged as

the vertices of a hexagon. To obtain $S(\mathbf{k}_{||})$ collected images were shifted by their respective $k_{\mathrm{in},||}$, while overlapping image areas were averaged.

Absorption measurements

Absorption measurements on the membrane were done by using an integrating sphere microscope (modified LabSphere GPS-020-SL with the 17 mm working distance objective Mitutoyo M Apo Plan NIR 50× and NA = 0.42) coupled with a supercontinuum laser (Fianium WL-SC-390-3) and an acousto-optical tunable filter (AOTF, Crystal Technologies, with roughly 4 nm bandwidth). The back-scattered and transmitted light are both detected together and by adding the specularly reflected signal, we determine absorption. The photodetectors are Thorlabs amplified Si detectors (PDA100A), read out by Stanford Research Systems SR830 lock-in amplifiers. More details about the integrating sphere microscope set-up can be found in Ref. 52 . We have used three photo-detectors to measure the reference beam, the reflected and the transmitted/forward scattered light, respectively. The light reflected back into the objective is detected with the reflection detector, while the integrating sphere detector detects the transmitted and scattered light. The absorbance is calculated by subtracting the reflected and transmitted/scattered power from the incident power. Two reference measurements in reflection and transmission were done with a glass slide and calibrated mirror, to account for the response function of the set-up.

Acknowledgement

This work is part of the Dutch Research Council (NWO) and was partially performed at the research institute AMOLF. R.S. acknowledges funding by EPSRC (EP/P033431, EP/M013812 and EP/M027961). M.F. acknowledges support from the University of Surrey's IAA awards, the EPSRC (United Kingdom) EP/N509772/1, EPSRC (United Kingdom) Strategic Equipment Grant No. EP/L02263X/1 (EP/M008576/1) and EPSRC (United

Kingdom) Grant EP/M027791/1.

The authors thank Julia van der Burgt and Albert Polman for fruitful discussions. Special thanks also to the technical support staff of the AMOLF NanoLab Amsterdam, for their support with sample fabrication.

Author contributions

R.J.S., G.G. C.W. and M.F. carried out the HUD optimisation and optical simulations. N.T., E.K. and R. R. performed the measurements and processed the experimental data. P.K. performed the PC1D simulations. E.A.L., R.S., M.F. and A.F.K. were involved in planning and supervision of the work. E.A.L. and M.F. initiated and directed the project. All authors contributed to writing the manuscript.

Supporting Information Available

A listing of the contents of the Supporting Information file is below:

- Design parameters
- Absorption spectra in the full device
- Silicon dispersion model
- Mode coupling analysis
- Angular dependence of absorption
- PC1D simulation details
- Bulk lifetime and surface recombination effects

References

(1) Liu, Z.; Sofia, S. E.; Laine, H. S.; Woodhouse, M.; Wieghold, S.; Peters, I. M.; Buonassisi, T. Revisiting thin silicon for photovoltaics: A technoeconomic perspective. *Energy Environ. Sci.* **2020**, *13*, 12–23.

(2) Fedorchenko, A. I.; Wang, A. B.; Cheng, H. H. Thickness dependence of nanofilm elastic modulus. *Appl. Phys. Lett.* **2009**, *94*, 152111.

(3) Wang, S.; Weil, B. D.; Li, Y.; Wang, K. X.; Garnett, E.; Fan, S.; Cui, Y. Large-area free-standing ultrathin single-crystal silicon as processable materials. *Nano Lett.* **2013**, *13*, 4393–4398.

(4) Bong, J. H.; Kim, C.; Hwang, W. S.; Kim, T. S.; Cho, B. J. A quantitative strain analysis of a flexible single-crystalline silicon membrane. *Appl. Phys. Lett.* **2017**, *110*, 033105.

(5) Richter, A.; Hermle, M.; Glunz, S. W. Reassessment of the limiting efficiency for crystalline silicon solar cells. *IEEE J. Photovoltaics* **2013**, *3*, 1184–1191.

(6) Kowalczewski, P.; Andreani, L. C. Towards the efficiency limits of silicon solar cells: How thin is too thin? *Sol. Energy Mater. Sol. Cells* **2015**, *143*, 260–268.

(7) Polman, A.; Atwater, H. A. Photonic design principles for ultrahigh-efficiency photovoltaics. *Nat. Mater.* **2012**, *11*, 174–177.

(8) Pala, R. A.; White, J.; Barnard, E.; Liu, J.; Brongersma, M. L. Design of plasmonic thin-film solar cells with broadband absorption enhancements. *Adv. Mater.* **2009**, *21*, 3504–3509.

(9) Yu, P.; Zhang, F.; Li, Z.; Zhong, Z.; Govorov, A.; Fu, L.; Tan, H.; Jagadish, C.; Wang, Z. Giant optical pathlength enhancement in plasmonic thin film solar cells using core-shell nanoparticles. *J. Phys. D. Appl. Phys.* **2018**, *51*, 295106.

(10) Raja, W.; Bozzola, A.; Zilio, P.; Miele, E.; Panaro, S.; Wang, H.; Toma, A.; Alabastri, A.; De Angelis, F.; Zaccaria, R. P. Broadband absorption enhancement in plasmonic nanoshells-based ultrathin microcrystalline-Si solar cells. *Sci. Rep.* **2016**, *6*, 24539.

(11) Ferry, V. E.; Sweatlock, L. A.; Pacifici, D.; Atwater, H. A. Plasmonic Nanostructure Design for Efficient Light Coupling into Solar Cells. *Nano Lett.* **2008**, *8*, 4391–4397.

(12) Chen, H.-L.; Cattoni, A.; De Lépinau, R.; Walker, A. W.; Höhn, O.; Lackner, D.; Siefer, G.; Faustini, M.; Vandamme, N.; Goffard, J.; Behaghel, B.; Dupuis, C.; Bardou, N.; Dimroth, F.; Collin, S. A 19.9%-efficient ultrathin solar cell based on a 205-nm-thick GaAs absorber and a silver nanostructured back mirror. *Nat. Energy* **2019**, *4*, 761–767.

(13) Gomard, G.; Drouard, E.; Letartre, X.; Meng, X.; Kaminski, A.; Fave, A.; Lemiti, M.; Garcia-Caurel, E.; Seassal, C. Two-dimensional photonic crystal for absorption enhancement in hydrogenated amorphous silicon thin film solar cells. *J. Appl. Phys.* **2010**, *108*, 123102.

(14) Battaglia, C.; Hsu, C. M.; Söderström, K.; Escarré, J.; Haug, F. J.; Charrière, M.; Boccard, M.; Despeisse, M.; Alexander, D. T.; Cantoni, M.; Cui, Y.; Ballif, C. Light trapping in solar cells: Can periodic beat random? *ACS Nano* **2012**, *6*, 2790–2797.

(15) Yin, G.; Knight, M. W.; van Lare, M. C.; Solà Garcia, M. M.; Polman, A.; Schmid, M. Optoelectronic Enhancement of Ultrathin CuIn1–xGaxSe2 Solar Cells by Nanophotonic Contacts. *Adv. Opt. Mater.* **2017**, *5*, 1600637.

(16) Jäger, K.; Fischer, M.; van Swaaij, R. A. C. M. M.; Zeman, M. A scattering model for nano-textured interfaces and its application in opto-electrical simulations of thin-film silicon solar cells. *J. Appl. Phys.* **2012**, *111*, 083108.

(17) Martins, E. R.; Li, J.; Liu, Y.; Depauw, V.; Chen, Z.; Zhou, J.; Krauss, T. F. De-

terministic quasi-random nanostructures for photon control. *Nat. Commun.* **2013**, *4*, 2665.

(18) Vynck, K.; Burresi, M.; Riboli, F.; Wiersma, D. S. Photon management in two-dimensional disordered media. *Nat. Mater.* **2012**, *11*, 1017–1022.

(19) Oskooi, A.; Favuzzi, P. A.; Tanaka, Y.; Shigeta, H.; Kawakami, Y.; Noda, S. Partially disordered photonic-crystal thin films for enhanced and robust photovoltaics. *Appl. Phys. Lett.* **2012**, *100*, 181110.

(20) Ferry, V. E.; Verschuuren, M. A.; Lare, M. C. V.; Schropp, R. E.; Atwater, H. A.; Polman, A. Optimized spatial correlations for broadband light trapping nanopatterns in high efficiency ultrathin film a-Si:H solar cells. *Nano Lett.* **2011**, *11*, 4239–4245.

(21) Van Lare, C.; Lenzmann, F.; Verschuuren, M. A.; Polman, A. Dielectric Scattering Patterns for Efficient Light Trapping in Thin-Film Solar Cells. *Nano Lett.* **2015**, *15*, 4846–4852.

(22) Yu, S.; Wang, C.; Zhang, Y.; Dong, B.; Jiang, Z.; Chen, X.; Chen, W.; Sun, C. Design of Non-Deterministic Quasi-random Nanophotonic Structures Using Fourier Space Representations. *Sci. Rep.* **2017**, *7*, 3752.

(23) Pratesi, F.; Burresi, M.; Riboli, F.; Vynck, K.; Wiersma, D. S. Disordered photonic structures for light harvesting in solar cells. *Opt. Express* **2013**, *21*, A460.

(24) Siddique, R. H.; Donie, Y. J.; Gomard, G.; Yalamanchili, S.; Merdzhanova, T.; Lemmer, U.; Hölscher, H. Bioinspired phase-separated disordered nanostructures for thin photovoltaic absorbers. *Sci. Adv.* **2017**, *3*, e1700232.

(25) Bozzola, A.; Liscidini, M.; Andreani, L. C. Broadband light trapping with disordered photonic structures in thin-film silicon solar cells. *Prog. Photovoltaics Res. Appl.* **2014**, *22*, 1237–1245.

(26) Trevino, J.; Forestiere, C.; Di Martino, G.; Yerci, S.; Priolo, F.; Dal Negro, L. Plasmonic-photonic arrays with aperiodic spiral order for ultra-thin film solar cells. *Opt. Express* **2012**, *20*, A418.

(27) Torquato, S.; Stillinger, F. H. Local density fluctuations, hyperuniformity, and order metrics. *Phys. Rev. E - Stat. Physics, Plasmas, Fluids, Relat. Interdiscip. Top.* **2003**, *68*, 41113.

(28) Uche, O. U.; Stillinger, F. H.; Torquato, S. Constraints on collective density variables: Two dimensions. *Phys. Rev. E - Stat. Physics, Plasmas, Fluids, Relat. Interdiscip. Top.* **2004**, *70*, 9.

(29) Batten, R. D.; Stillinger, F. H.; Torquato, S. Classical disordered ground states: Super-ideal gases and stealth and equi-luminous materials. *J. Appl. Phys.* **2008**, *104*, 33504.

(30) Castro-Lopez, M.; Gaio, M.; Sellers, S.; Gkantzounis, G.; Florescu, M.; Sapienza, R. Reciprocal space engineering with hyperuniform gold disordered surfaces. *APL Photon.* **2017**, *2*, 174–7.

(31) Gabrielli, A.; Labini, F. S.; Joyce, M.; Pietronero, L. *Stat. Phys. Cosm. Struct.*; Springer-Verlag: Berlin/Heidelberg, 2005; pp 1–424.

(32) Zhang, G.; Martelli, F.; Torquato, S. The structure factor of primes. *J. Phys. A Math. Theor.* **2018**, *51*, 115001.

(33) Lei, Q. L.; Ni, R. Hydrodynamics of random-organizing hyperuniform fluids. *PNAS* **2019**, *116*, 22983–22989.

(34) Mann, S. A.; Sciacca, B.; Zhang, Y.; Wang, J.; Kontoleta, E.; Liu, H.; Garnett, E. C. Integrating Sphere Microscopy for Direct Absorption Measurements of Single Nanostructures. *ACS Nano* **2017**, *11*, 1412–1418.

(35) Wang, J.; Schwarz, J. M.; Paulsen, J. D. Hyperuniformity with no fine tuning in sheared sedimenting suspensions. *Nat. Commun.* **2018**, *9*, 1–7.

(36) Froufe-Pérez, L. S.; Engel, M.; Sáenz, J. J.; Scheffold, F. Band gap formation and Anderson localization in disordered photonic materials with structural correlations. *PNAS* **2017**, *114*, 9570–9574.

(37) Ricouvier, J.; Pierrat, R.; Carminati, R.; Tabeling, P.; Yazhgur, P. Optimizing Hyperuniformity in Self-Assembled Bidisperse Emulsions. *Phys. Rev. Lett.* **2017**, *119*, 208001.

(38) Florescu, M.; Torquato, S.; Steinhardt, P. J. Designer disordered materials with large, complete photonic band gaps. *PNAS* **2009**, *106*, 20658–20663.

(39) Froufe-Pérez, L. S.; Engel, M.; Damasceno, P. F.; Muller, N.; Haberko, J.; Glotzer, S. C.; Scheffold, F. Role of Short-Range Order and Hyperuniformity in the Formation of Band Gaps in Disordered Photonic Materials. *Phys. Rev. Lett.* **2016**, *117*, 053902.

(40) Tsitrin, S.; Williamson, E. P.; Amoah, T.; Nahal, G.; Chan, H. L.; Florescu, M.; Man, W. Unfolding the band structure of non-crystalline photonic band gap materials. *Sci. Rep.* **2015**, *5*, 13301.

(41) Leseur, O.; Pierrat, R.; Carminati, R. High-density hyperuniform materials can be transparent. *Optica* **2016**, *3*, 763–767.

(42) Gorsky, S.; Britton, W. A.; Chen, Y.; Montaner, J.; Lenef, A.; Raukas, M.; Dal Negro, L. Engineered hyperuniformity for directional light extraction. *APL Photon.* **2019**, *4*, 110801.

(43) Milošević, M. M.; Man, W.; Nahal, G.; Steinhardt, P. J.; Torquato, S.; Chaikin, P. M.; Amoah, T.; Yu, B.; Mullen, R. A.; Florescu, M. Hyperuniform disordered waveguides and devices for near infrared silicon photonics. *Sci. Rep.* **2019**, *9*, 1–11.

(44) Man, W.; Florescu, M.; Williamson, E. P.; He, Y.; Hashemizad, S. R.; Leung, B. Y.; Liner, D. R.; Torquato, S.; Chaikin, P. M.; Steinhardt, P. J. Isotropic band gaps and freeform waèeguides obserèed in hyperuniform disordered photonic solids. *PNAS* **2013**, *110*, 15886–15891.

(45) Amoah, T.; Florescu, M. High- Q optical cavities in hyperuniform disordered materials. *Phys. Rev. B - Condens. Matter Mater. Phys.* **2015**, *91*, 020201.

(46) Ma, T.; Guerboukha, H.; Girard, M.; Squires, A. D.; Lewis, R. A.; Skorobogatiy, M. 3D Printed Hollow-Core Terahertz Optical Waveguides with Hyperuniform Disordered Dielectric Reflectors. *Adv. Opt. Mater.* **2016**, *4*, 2085–2094.

(47) Zhou, W.; Tong, Y.; Sun, X.; Tsang, H. K. Hyperuniform disordered photonic bandgap polarizers. *J. Appl. Phys.* **2019**, *126*, 113106.

(48) PALIK, E. D., Ed. *Handb. Opt. Constants Solids*; Academic Press: Boston, 1998; p iii.

(49) Ghiradella, H. Light and color on the wing: structural colors in butterflies and moths. *Appl. Opt.* **1991**, *30*, 3492.

(50) Gissibl, T.; Wagner, S.; Sykora, J.; Schmid, M.; Giessen, H. Refractive index measurements of photo-resists for three-dimensional direct laser writing. *Opt. Mater. Express* **2017**, *7*, 2293.

(51) Mann, S. A.; Oener, S. Z.; Cavalli, A.; Haverkort, J. E.; Bakkers, E. P.; Garnett, E. C. Quantifying losses and thermodynamic limits in nanophotonic solar cells. *Nat. Nanotech.* **2016**, *11*, 1071–1075.

(52) Mann, S. A.; Sciacca, B.; Zhang, Y.; Wang, J.; Kontoleta, E.; Liu, H.; Garnett, E. C. Integrating Sphere Microscopy for Direct Absorption Measurements of Single Nanostructures. *ACS Nano* **2017**, *11*, 1412–1418.

(53) Depauw, V.; Trompoukis, C.; Massiot, I.; Chen, W.; Dmitriev, A.; Roca I Cabarrocas, P.; Gordon, I.; Poortmans, J. Sunlight-thin nanophotonic monocrystalline silicon solar cells. *Nano Futur.* **2017**, *1*, 021001.

(54) Bozzola, A.; Liscidini, M.; Andreani, L. C. Broadband light trapping with disordered photonic structures in thin-film silicon solar cells. *Prog. Photovolt: Res. Appl.* **2014**, *22*, 1237–1245.

(55) Li, J.; Li, K.; Schuster, C.; Su, R.; Wang, X.; Borges, B. H. V.; Krauss, T. F.; Martins, E. R. Spatial resolution effect of light coupling structures. *Sci. Rep.* **2015**, *5*, 18500.

(56) Hejna, M.; Steinhardt, P. J.; Torquato, S. Nearly hyperuniform network models of amorphous silicon. *Phys. Rev. B - Condens. Matter Mater. Phys.* **2013**, *87*, 245204.

(57) Schokker, A. H.; Koenderink, A. F. Lasing at the band edges of plasmonic lattices. *Phys. Rev. B - Condens. Matter Mater. Phys.* **2014**, *90*, 155452.

(58) Teubner, M. Level Surfaces of Gaussian Random Fields and Microemulsions. *Europhys. Lett.* **1991**, *14*, 403–408.

(59) Ma, Z.; Torquato, S. Random scalar fields and hyperuniformity. *J. Appl. Phys.* **2017**, *121*, 244904.

(60) Yoshikawa, K.; Kawasaki, H.; Yoshida, W.; Irie, T.; Konishi, K.; Nakano, K.; Uto, T.; Adachi, D.; Kanematsu, M.; Uzu, H.; Yamamoto, K. Silicon heterojunction solar cell with interdigitated back contacts for a photoconversion efficiency over 26%. *Nat. Energy* **2017**, *2*, 1–8.

(61) Jeong, S.; McGehee, M. D.; Cui, Y. All-back-contact ultra-thin silicon nanocone solar cells with 13.7% power conversion efficiency. *Nat. Commun.* **2013**, *4*, 1–7.

(62) Tomasi, A.; Paviet-Salomon, B.; Jeangros, Q.; Haschke, J.; Christmann, G.; Barraud, L.; Descoeudres, A.; PeterSeif, J.; Nicolay, S.; Despeisse, M.; De Wolf, S.; Ballif, C. Simple processing of back-contacted silicon heterojunction solar cells using selective-area crystalline growth. *Nat. Energy* **2017**, *2*, 17062.

(63) Sai, H.; Umishio, H.; Matsui, T.; Nunomura, S.; Kawatsu, T.; Takato, H.; Matsubara, K. Impact of silicon wafer thickness on photovoltaic performance of crystalline silicon heterojunction solar cells. Jpn. J. Appl. Phys. 2018.

(64) Bläsi, B.; Tucher, N.; Höhn, O.; Kübler, V.; Kroyer, T.; Wellens, C.; Hauser, H. Large area patterning using interference and nanoimprint lithography. *Micro-Optics 2016* **2016**, *9888*, 98880H.

(65) Donie, Y. J.; Smeets, M.; Egel, A.; Lentz, F.; Preinfalk, J. B.; Mertens, A.; Smirnov, V.; Lemmer, U.; Bittkau, K.; Gomard, G. Light trapping in thin film silicon solar cells: Via phase separated disordered nanopillars. *Nanoscale* **2018**, *10*, 6651–6659.

(66) Piechulla, P. M.; Muehlenbein, L.; Wehrspohn, R. B.; Nanz, S.; Abass, A.; Rockstuhl, C.; Sprafke, A. Fabrication of Nearly-Hyperuniform Substrates by Tailored Disorder for Photonic Applications. *Adv. Opt. Mater.* **2018**, *6*, 1–10.

(67) Salvalaglio, M.; Bouabdellaoui, M.; Bollani, M.; Benali, A.; Favre, L.; Claude, J.-B.; Wenger, J.; de Anna, P.; Intonti, F.; Voigt, A.; Abbarchi, M. Hyperuniform monocrystalline structures by spinodal solid-state dewetting. 2019.

(68) Verschuuren, M. A.; Knight, M. W.; Megens, M.; Polman, A. Nanoscale spatial limitations of large-area substrate conformal imprint lithography. *Nanotech.* **2019**, *30*, 345301.

(69) Oskooi, A. F.; Roundy, D.; Ibanescu, M.; Bermel, P.; Joannopoulos, J. D.; Johnson, S. G. Meep: A flexible free-software package for electromagnetic simulations by the FDTD method. *Computer Physics Communications* **2010**, *181*, 687–702.

(70) Davis, J. A.; Cottrell, D. M.; Campos, J.; Yzuel, M. J.; Moreno, I. Encoding amplitude information onto phase-only filters. *Appl. Opt.* **1999**, *38*, 5004.